Physics Letters B 772 (2017) 599–606

Contents lists available at ScienceDirect

Physics Letters B

www.elsevier.com/locate/physletb

# Enhanced collectivity along the $N = Z$ line: Lifetime measurements in $^{44}$Ti, $^{48}$Cr, and $^{52}$Fe

K. Arnswald [a,*], T. Braunroth [a], M. Seidlitz [a], L. Coraggio [b], P. Reiter [a], B. Birkenbach [a], A. Blazhev [a], A. Dewald [a], C. Fransen [a], B. Fu [a], A. Gargano [b], H. Hess [a], R. Hirsch [a], N. Itaco [b,c], S.M. Lenzi [d], L. Lewandowski [a], J. Litzinger [a], C. Müller-Gatermann [a], M. Queiser [a], D. Rosiak [a], D. Schneiders [a], B. Siebeck [a], T. Steinbach [a], A. Vogt [a], K. Wolf [a], K.O. Zell [a]

[a] Institut für Kernphysik, Universität zu Köln, Zülpicher Straße 77, D-50937 Köln, Germany
[b] Istituto Nazionale di Fisica Nucleare, Sezione di Napoli, I-80126 Napoli, Italy
[c] Dipartimento di Matematica e Fisica, Università degli Studi della Campania "Luigi Vanvitelli", Viale A. Lincoln 5, I-8110 Caserta, Italy
[d] Dipartimento di Fisica dell'Università and INFN, Sezione di Padova, I-35141 Padova, Italy

ARTICLE INFO

*Article history:*
Received 8 May 2017
Received in revised form 29 June 2017
Accepted 15 July 2017
Available online 20 July 2017
Editor: V. Metag

*Keywords:*
$N = Z$ nuclei
Lifetime measurements
RDDS
$B$(E2) values

ABSTRACT

Lifetimes of the $2_1^+$ states in $^{44}$Ti, $^{48,50}$Cr, and $^{52}$Fe were determined with high accuracy exploiting the recoil distance Doppler-shift method. The reduced E2 transition strengths of $^{44}$Ti and $^{52}$Fe differ considerably from previously known values. A systematic increase in collectivity is found for the $N = Z$ nuclei compared to neighboring isotopes. The $B$(E2) values along the Ti, Cr, and Fe isotopic chains are compared to shell-model calculations employing established interactions for the $0f1p$ shell, as well as a novel effective shell-model Hamiltonian starting from a realistic nucleon–nucleon potential. The theoretical approaches underestimate the $B$(E2) values for the lower-mass Ti isotopes. Strong indication is found for particle-hole cross-shell configurations, recently corroborated by similar results for the neighboring isotone $^{42}$Ca.



## 1. Introduction

Reduced transition strengths are sensitive observables to study the properties of atomic nuclei and the evolution of nuclear structure. A basic indicator for the collectivity and for the shape of even–even nuclei is given by the $B$(E2) values especially for the excited $2_1^+$ states. Together with the transition strengths of the $4_1^+$ states, the vibrational or rotational character of the individual isotopes can be deduced. The measurement of the reduced transition probability of the $2_1^+ \rightarrow 0_{g.s.}^+$ transition in the $N = Z$ nuclei $^{44}$Ti, $^{48}$Cr, and $^{52}$Fe allows to delineate the evolution of the quadrupole collectivity between the doubly-magic shell closures at $N = Z = 20$ and $N = Z = 28$ where deviations from the spherical shape and its vibrational character are of high interest. Existing experimental results feature puzzling peculiarities with respect to the properties of excited $2_1^+$ and $4_1^+$ states in these nuclei and motivated the following investigations.

For the neutron-deficient Ti isotopes the $B(E2; 2_1^+ \rightarrow 0_{g.s.}^+)$ value for $^{44}$Ti [1–3] appeared to be significantly smaller than the respective $B$(E2) value in the neighboring semi-magic $N = 20$ isotope $^{42}$Ti [4] (cf. Fig. 1). This observation contradicts the general expectation and would question the robustness of the $N = 20$ shell closure for Ti. Moreover, other experimental studies of $^{44}$Ti showed a rotational-like excitation-energy spacing on top of the excited $0_2^+$ state [5]. Theoretical predictions concur with this observation and claim highly-deformed $12p$–$8h$ and $16p$–$12h$ configurations at 12 MeV and 20 MeV, respectively, as origin of these bands [6]. Recently, shape parameters in the isotone $^{42}$Ca were determined from a Coulomb-excitation experiment [7]. As a result, a weakly-deformed ground-state band and a slightly triaxial superdeformed sideband were discovered. Especially, the observed enhanced quadrupole deformation of the $2_1^+$ state suggests a possible mixing with the superdeformed $2_2^+$ state. An intriguing question is related to the $N = Z$ isotonic neighbor $^{44}$Ti where a similar

* Corresponding author.
*E-mail address:* konrad.arnswald@ikp.uni-koeln.de (K. Arnswald).

http://dx.doi.org/10.1016/j.physletb.2017.07.032

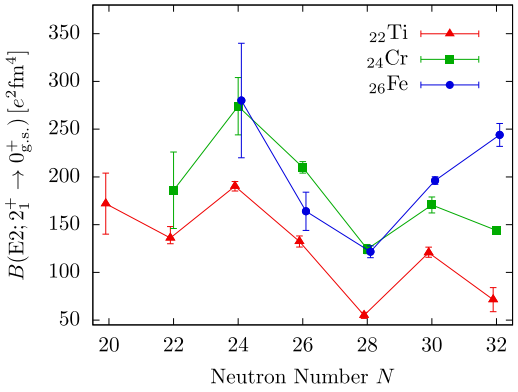


**Fig. 1.** (Color online.) Previously known $B(E2; 2_1^+ \rightarrow 0^+_{g.s.})$ values of Ti (red triangles), Cr (green squares), and Fe (blue circles) isotopes. Adopted $B(E2)$ values are taken from Ref. [8]. For $^{56}$Cr recent results from Ref. [9] are additionally considered. For better visibility, the data points of the same element are connected and the Ti and Fe chains are slightly shifted horizontally with respect to the Cr data.

structure can be expected. From the interplay between deformed and highly-deformed sidebands and the yrast $2^+$ state, like in $^{42}$Ca, a clearly enhanced $B(E2; 2_1^+ \rightarrow 0^+_{g.s.})$ value is anticipated for $^{44}$Ti in contradiction to the experimental results.

In addition, the ratio of reduced transition strengths $B_{4/2} = B(E2; 4_1^+ \rightarrow 2_1^+)/B(E2; 2_1^+ \rightarrow 0^+_{g.s.})$ was exploited in Refs. [2,10] to characterize the nuclei $^{44}$Ti, $^{48}$Cr and $^{52}$Fe. The values indicate a rapid change from a vibrational behavior for $^{44}$Ti and $^{52}$Fe to an extreme single-particle value at mid-shell for $^{48}$Cr. However, the ratios are subject to large experimental uncertainties.

The lifetime of the $2_1^+$ state in $^{48}$Cr was addressed by several experiments using early recoil distance Doppler-shift measurements after fusion-evaporation reactions [11–13]. A maximum $B(E2)$ value was measured at the $f_{7/2}$ mid-shell position. However, large experimental uncertainties motivated the improved experiments of this publication.

The $B(E2)$ value of the ground-state transition in $^{52}$Fe was deduced from a recent Coulomb-excitation experiment at intermediate energies at the National Superconducting Cyclotron Laboratory employing the SeGA detector array [14]. A moderate increase of quadrupole collectivity was found with respect to the neighboring shell closure at the $N = 28$ isotope $^{54}$Fe. A complementary approach, based on the RDDS technique, was employed in the new experiment to determine the lifetime of the corresponding $2_1^+$ state in $^{52}$Fe. A summary of the previously known experimental $B(E2; 2_1^+ \rightarrow 0^+_{g.s.})$ values is shown in Fig. 1 for the Ti, Cr, and Fe isotopes from $N = 20$ to 32.

From theoretical point of view, the $0f1p$ shell nuclei provide an excellent testing ground for modern shell-model calculations. The following three shell-model interactions FPD6 [15], KB3G [16], and GXPF1A [17] were developed in part by fitting experimental data of the nuclei of interest and are thus suited to describe the envisaged region of the nuclear chart. Detailed new calculations are subject of this letter. Moreover, a new effective shell-model Hamiltonian starting from a realistic nucleon–nucleon potential was employed in order to describe the experimental findings.

As protons and neutrons occupy the same major shell, the neutron–proton interaction becomes important, enhancing collective effects like isoscalar ($T = 0$) neutron–proton pairing. Theoretical investigations on $T = 0$ ground-state correlations were performed for $^{44}$Ti [18]. Furthermore, results from Ref. [19] indicate that for $N = Z = 24$ ($^{48}$Cr) neutron–proton pair correlations become important at higher spin values. Isoscalar neutron–proton pairing is even more relevant for heavier, exotic $N = Z$ nuclei towards doubly-magic $^{100}$Sn [18,20]. For example, it is expected that the self-conjugate $^{88}$Ru has a significantly enhanced E2 transition strength [21]. A recent study in the neighboring $N = Z = 46$ nucleus $^{92}$Pd revealed experimental evidence for $T = 0$ neutron–proton pairing [22].

A different theoretical approach exploits the $\alpha$-cluster structure in the $fp$-shell region where a strong spin-orbit force is counteracting the $\alpha$ correlations. However, the observation of an $\alpha$-cluster band in $^{44}$Ti confirmed the applicability of the $\alpha$-cluster model. Detailed theoretical $B(E2)$ values are available for $^{44}$Ti from Ref. [23] which show a considerably enhanced collective behavior. A refined theoretical study in this line exploits deformed-basis antisymmetrized molecular dynamics (AMD) by the use of the Gogny D1S force [24] and yield coexistence phenomena in $^{44}$Ti. A mixed character of the mean-field-like structure and the $\alpha + {}^{40}$Ca cluster structure of the yrast band in $^{44}$Ti is obtained implying a high $B(E2; 2_1^+ \rightarrow 0^+_{g.s.})$ value. These results are given in Ref. [24] and exceed the previously measured $B(E2)$ value [1–3].

A new experimental investigation is motivated by the fact that the lifetime of the $2_1^+$ state in $^{44}$Ti is mainly known from pioneering studies performed in the 1970's with limited precision [1,2]. The same is true for the $2_1^+$ state in $^{48}$Cr which was addressed by earlier experiments [11–13]. The determined lifetime values were given with considerable error bars. Nowadays, the recoil distance Doppler-shift (RDDS) method has proven to provide precise, reliable, and model-independent lifetime values in the picosecond range for excited nuclear states. The method is applicable for stable-beam experiments as well as for the measurement of transition strengths in exotic nuclei [9,25–28].

A measurement of the reduced transition strengths with increased precision for the $N = Z$ nuclei $^{44}$Ti, $^{48}$Cr, and $^{52}$Fe was performed to address the open questions and puzzling observations. Nuclear level lifetimes in the isotopes of interest were studied employing the RDDS techniques with stable ion beams, which allows high accuracy by exploitation of $\gamma\gamma$-correlation gated spectra and by elimination of systematic errors like unobserved side-feeding effects.

## 2. Experiment

Three experiments were performed at the FN tandem accelerator at the Institute for Nuclear Physics, University of Cologne, combining a setup of twelve high-purity germanium (HPGe) detectors and the Cologne coincidence-plunger device [29]. Excited states in the nuclei of interest were populated by the following fusion-evaporation reactions: $^{nat.}$Mg($^{23}$Na, $x$np)$^{44}$Ti, $^{40}$Ca($^{10}$B, np)$^{48}$Cr, and $^{27}$Al($^{28}$Si, 2np)$^{52}$Fe.

The plunger targets were made of $^{nat.}$Mg ($^{40}$Ca, $^{27}$Al) with a thickness of 1 mg/cm$^2$ (0.50 mg/cm$^2$, 0.58 mg/cm$^2$) for the $^{44}$Ti ($^{48}$Cr, $^{52}$Fe) recoils. While the magnesium target was self-supporting, the calcium and aluminum target material was evaporated onto a 2.0-mg/cm$^2$ gold backing facing the beam. The calcium target was additionally protected against oxidation by a 0.1-mg/cm$^2$ gold layer. Recoiling nuclei left the target with 2.7% (1.1%, 3.1%) of the speed of light which corresponds to mean velocities of 8.1 µm/ps (3.3 µm/ps, 9.3 µm/ps). Reaction products were finally stopped in a 9.6-mg/cm$^2$ thick gold foil. During the experiment data were recorded at 6 (12, 7) different target-to-stopper distances, i.e. different flight times of the recoiling nuclei. These distances reach from 21.5 to 47.5 µm (20.4 to 321 µm, 28.6 to 151.6 µm) and were measured with an accuracy of better than 2%. Beam-depending changes, such as thermal expansion of the target, were compensated by a feedback system employing a piezoelectric linear motor. The experimental details are summarized in Table 1.

Emitted $\gamma$ rays were detected by twelve HPGe detectors with relative efficiencies between 55% and 80% which were placed in

**Table 1**
Experimental details: Reactions, target properties, and offset-corrected relative target-to-stopper distances of the plunger device for each of the three experiments.

| Reaction | $E_{beam}$ [MeV] | Target thickness [mg/cm$^2$] | Recoil velocity [μm/ps] | Target-to-stopper distances | Target-to-stopper range [μm] |
|---|---|---|---|---|---|
| $^{nat.}$Mg($^{23}$Na, $x$np)$^{44}$Ti | 62 | 1 | 8.1(4) | 6 | 21.5–47.5 |
| $^{40}$Ca($^{10}$B, np)$^{48}$Cr | 26 | 0.50 | 3.3(2) | 12 | 20.4–321 |
| $^{27}$Al($^{28}$Si, 2np)$^{52}$Fe | 86 | 0.58 | 9.3(4) | 7 | 28.6–151.6 |

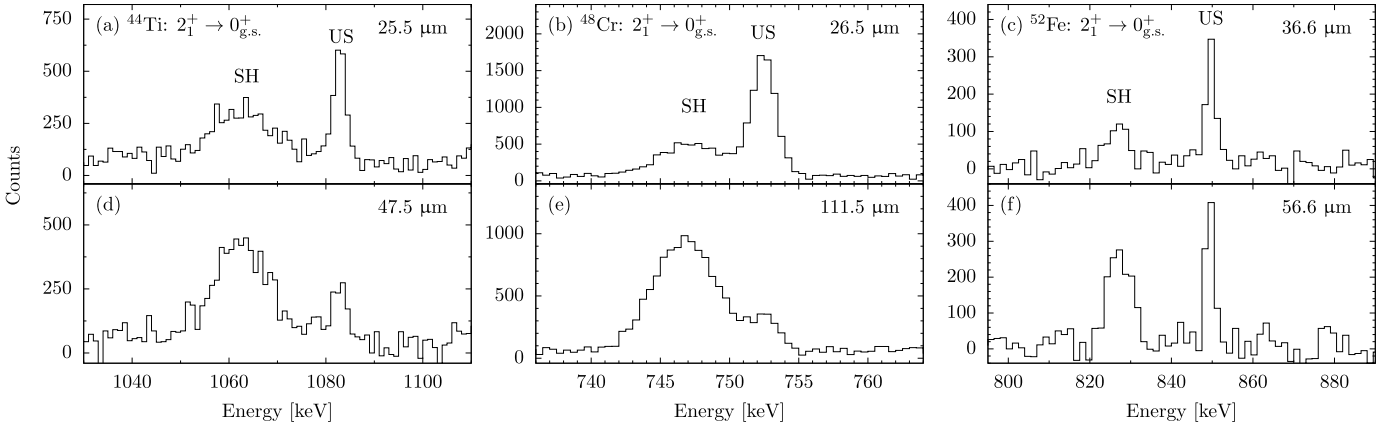


**Fig. 2.** Exemplary $\gamma$-ray energy spectra from the $2_1^+ \rightarrow 0_{g.s.}^+$ decay at (a, d) 1083 keV in $^{44}$Ti, at (b, e) 752 keV in $^{48}$Cr, and at (c, f) 849 keV in $^{52}$Fe. Spectra are produced from cuts on the shifted component of the $4_1^+ \rightarrow 2_1^+$ transition and are shown for a short (a, b, c) and a larger (d, e, f) target-to-stopper distance at backward angles. Doppler-shifted (SH) components and unshifted (US) components are additionally labeled.

rings centered at polar angles of $\theta_0 = 0°$ (1 detector), $\theta_1 = 45°$ (6 detectors), and $\theta_2 = 143°$ (5 detectors) with respect to the beam axis. Each HPGe detector was shielded with sheets of lead and copper between target and endcap with a total thickness of 2 mm in order to reduce pile up and additional dead time caused by low-energy X rays. Furthermore, a hardware $\gamma\gamma$-coincidence trigger was used to suppress single $\gamma$-ray events, which do not contribute to the $\gamma\gamma$-coincidence analysis. Coincident $\gamma$-ray events were finally sorted into $\gamma\gamma$ matrices with respect to the different target-to-stopper distances and the correlation groups defined by the individual detector rings. The total statistics in the projected $\gamma\gamma$ matrices amount to $6.8 \times 10^9$ ($3.5 \times 10^9$, $7.3 \times 10^9$) events for the experiments to populate $^{44}$Ti, ($^{48}$Cr, and $^{52}$Fe), respectively.

## 3. Analysis and results

The lifetime analysis is based on the recoil distance Doppler-shift (RDDS) technique in conjunction with the differential decay-curve method (DDCM) [29]. Due to sufficient production yields of recoiling nuclei of interest, the DDCM was utilized in the $\gamma\gamma$-coincidence mode. Employing gates on the Doppler-shifted (SH) component of feeding transitions, or on the unshifted (US) part of the $2_1^+ \rightarrow 0_{g.s.}^+$ transitions, the lifetime of the $2_1^+$ states was determined by analyzing the intensity ratios of shifted and unshifted components of the depopulating and feeding transitions, respectively (cf. Fig. 2). A lifetime $\tau_i$ is deduced for each distance $i$ in the sensitive range. The $\tau$ curve is expected to be constant and the weighted mean value of the different $\tau_i$ corresponds to the analyzed lifetime. Lifetimes determined from different $\gamma\gamma$ matrices are statistically independent. The statistical uncertainty of the lifetime value is dominated by the distribution of the single $\tau_i$ values. Systematic errors of the lifetime arise from (i) the uncertainty of the recoil velocity which is inversely included in the lifetime value. The mean velocity was determined from the Doppler shift of the direct feeding transition observed at forward and backward angles. The uncertainty of the mean polar angle $\Delta\theta = 3°$ results in $\Delta\beta = 1.2 \times 10^{-3} (0.5 \times 10^{-3}, 1.3 \times 10^{-3})$ for $^{44}$Ti ($^{48}$Cr, $^{52}$Fe). (ii) The relative target-to-stopper distances can be measured with a high precision of $\Delta x \leq 0.4$ μm in the sensitive range. Thus, its contribution to the total uncertainty of $\tau$ was neglected. (iii) Contaminating transitions in the $\gamma\gamma$ coincidence gate may impact the experimental lifetimes. This was excluded in the analysis by the careful selection of narrow energy gates. Finally, the total systematic error of the lifetime was calculated via the Gaussian error propagation.

In the case of $^{44}$Ti a gate from below was set on the unshifted part of the $2_1^+ \rightarrow 0_{g.s.}^+$ transition at 1083 keV to avoid any background contribution in the region of interest. The lifetime of the $2_1^+$ state is finally determined from the shifted and the total intensities ($I_{SH}$ and $I_{SH+US}$) of the $4_1^+ \rightarrow 2_1^+$ feeding transition at 1371 keV and yields $\tau(2_1^+) = 2.68\,(21)_{stat.}\,(12)_{sys.}$ ps.

The $^{10}$B + $^{40}$Ca reaction caused a small Doppler shift for the $\gamma$ rays of interest in $^{48}$Cr due to a moderate momentum transfer. Therefore, the shifted and unshifted components of the $\gamma$-ray line are not separated completely from each other (see spectra in Figs. 2(b), (e)). To avoid any contamination of unshifted fractions in the selected gate, an indirect gate on the $8_1^+ \rightarrow 6_1^+$ transition at 1742 keV was used in the analysis. For this transition only a shifted component was observed indicating a fast behavior of the feeding structure (cf. Ref. [30]). Moreover, the low momentum transfer of the reaction and the large energy loss in the target result in a broad velocity distribution of the recoiling nuclei after the target, i.e. a wide range of flight times between target and stopper foil. Thus, the observed velocity distribution of the nuclei that emit a $\gamma$ ray in flight, depends on the target-to-stopper distance. A correction was applied which normalizes the distances to the observed maximum recoil velocities. The lifetime of the first $2^+$ state in $^{48}$Cr was determined from the feeding-corrected intensity distribution of the $2_1^+ \rightarrow 0_{g.s.}^+$ transition at 752 keV, which yields $\tau(2_1^+) = 12.16\,(14)_{stat.}\,(69)_{sys.}$ ps.

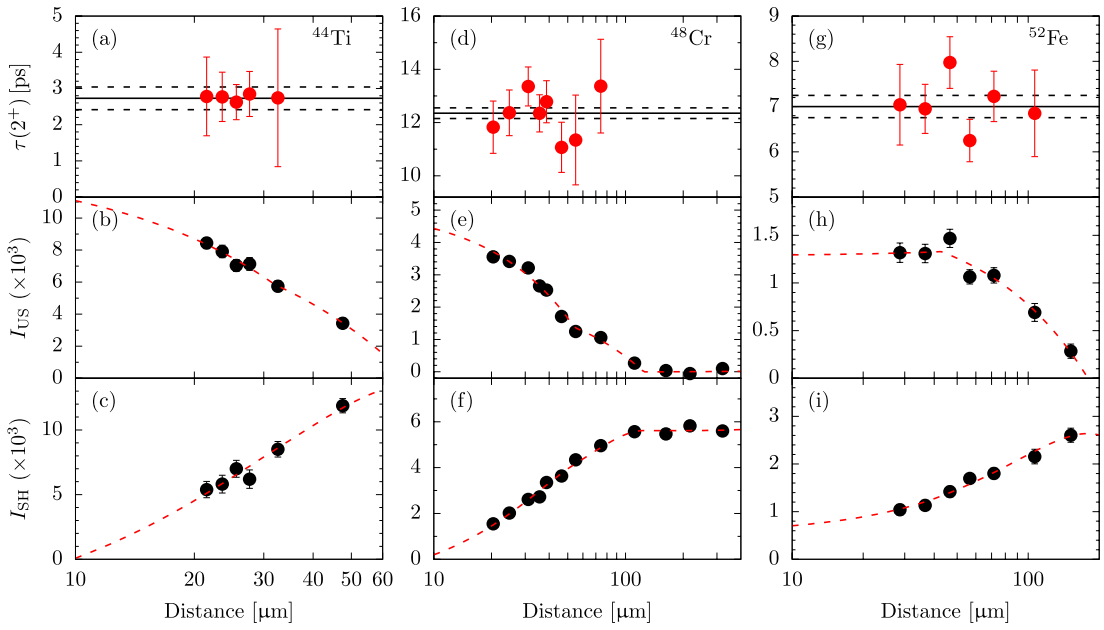


**Fig. 3.** (Color online.) $\tau$ curves of the $2_1^+$ states (a, d, g) are presented for the nuclei $^{44}$Ti, $^{48}$Cr, and $^{52}$Fe, respectively. Black solid lines indicate the weighted mean value of the lifetime; dashed lines mark the statistical uncertainty. Furthermore, the unshifted (b) and shifted (c) intensities of the direct populating transition in $^{44}$Ti are shown, as well as the unshifted intensities (e, h) and the shifted intensities (f, i) of the depopulating $2_1^+ \rightarrow 0_{g.s.}^+$ transition in $^{48}$Cr and $^{52}$Fe, respectively. The polynomial fit function to the given intensities is presented in dashed red. Lifetimes and $\gamma$-ray intensities are presented in dependence of the target-to-stopper distances. Note the logarithmic distance scale.

**Table 2**
Experimental lifetimes for the $2_1^+$ states in $^{44}$Ti, $^{48,50}$Cr, and $^{52}$Fe from the present experiment are compared to previous experimental values taken from Ref. [8,14]. The corresponding experimental and theoretical $B(E2; 2_1^+ \rightarrow 0_{g.s.}^+)$ values are included. The results are compared to four different shell-model calculations (for details see text).

| Nucleus | Experiment | | | | Theory | | | |
|---|---|---|---|---|---|---|---|---|
| | Lifetime [ps] | | $B(E2)$ [$e^2$ fm$^4$] | | $B(E2)$ [$e^2$ fm$^4$] | | | |
| | Present | Previous | Present | Previous | GXPF1A | KB3G | FPD6 | Realistic |
| $^{44}$Ti | 2.7(2) | $4.03^{+0.18}_{-0.32}$[a] | $205^{+20}_{-17}$ | $136^{+12}_{-6}$[a] | 105 | 119 | 140 | 120 |
| $^{48}$Cr | 12.2(7) | 12.4(14)[a] | $279^{+17}_{-15}$ | 274(30)[a] | 251 | 253 | 314 | 272 |
| $^{50}$Cr | 13.0(4) | $13.15^{+0.41}_{-0.29}$[a] | $214^{+7}_{-6}$ | 210(6)[a] | 218 | 218 | 276 | 243 |
| $^{52}$Fe | 7.0(4) | 11.3(14)[b] | $265^{+15}_{-13}$ | 163(20)[b] | 221 | 217 | 292 | 273 |

[a] From Ref. [8].
[b] Adapted from $B(E2; 0_{g.s.}^+ \rightarrow 2_1^+) = 817\,(102)\,e^2$ fm$^4$ in Ref. [14].

In $^{52}$Fe a narrow gate was applied to the shifted component of the $4_1^+ \rightarrow 2_1^+$ transition at 1535 keV. In the gated spectra a contaminant within the range of the shifted component of the $2_1^+ \rightarrow 0_{g.s.}^+$ transition at 849 keV obstructed a lifetime analysis in the forward detector rings. Therefore, the lifetime of the first $2^+$ state was determined using the upstream detector ring, yielding $\tau(2_1^+) = 7.00\,(24)_{stat.}\,(28)_{sys.}$ ps. In order to cross-check the modified analysis with only one detector-ring combination in $^{52}$Fe, an independent analysis of the lifetime of the $2_1^+$ state in the neighboring $^{50}$Cr was performed as a consistency check. This transition was observed with higher statistics and its analysis yields $\tau(2_1^+) = 13.0\,(3)_{stat.}\,(3)_{sys.}$ ps, which is in good agreement with the adopted lifetime of $\tau(2_1^+) = 13.15^{+0.41}_{-0.29}$ ps from Ref. [8].

The final $\tau$ curves of the $2_1^+$ states and the corresponding $\gamma$-ray intensities are presented for the nuclei $^{44}$Ti, $^{48}$Cr, and $^{52}$Fe in Fig. 3. Lifetime measurements of higher-lying yrast states were not feasible because these states are too short-lived for the applied target-to-stopper distances. Experimental results of measured lifetimes and corresponding $B(E2)$ values are summarized in Table 2. The final experimental error of the lifetime includes the root sum squared of the statistical and the systematic uncertainties.

## 4. Discussion

The measured lifetimes were converted into $B(E2; 2_1^+ \rightarrow 0_{g.s.}^+)$ values and are compared to previous experimental values (see Table 2). Results on $B(E2)$ values from new shell-model calculations were obtained and are also confronted with the new findings. Emphasize is given to the evolution along $N = Z$ and the respective even–even isotopic chains. The latter comparison is shown in Fig. 4 for the $2_1^+$ excitation energies (a, b, c) and the $B(E2)$ values (d, e, f).

The newly determined $2_1^+$ lifetime in $^{44}$Ti corresponds to a reduced transition probability $B(E2; 2_1^+ \rightarrow 0_{g.s.}^+) = 205^{+20}_{-17}\,e^2$ fm$^4$; while the adopted lifetime is $\tau = 4.03^{+0.18}_{-0.32}$ ps with $B(E2; 2_1^+ \rightarrow 0_{g.s.}^+) = 136^{+12}_{-6}\,e^2$ fm$^4$ [8]. Thus, there is a $4\sigma$ deviation between both values. The adopted value includes results deduced from lifetime experiments employing the Doppler-shift attenuation method (DSAM) following $\alpha$-capture and $\alpha$-transfer reactions on a $^{40}$Ca target [2,3]. For this type of experiments, systematic uncertainties

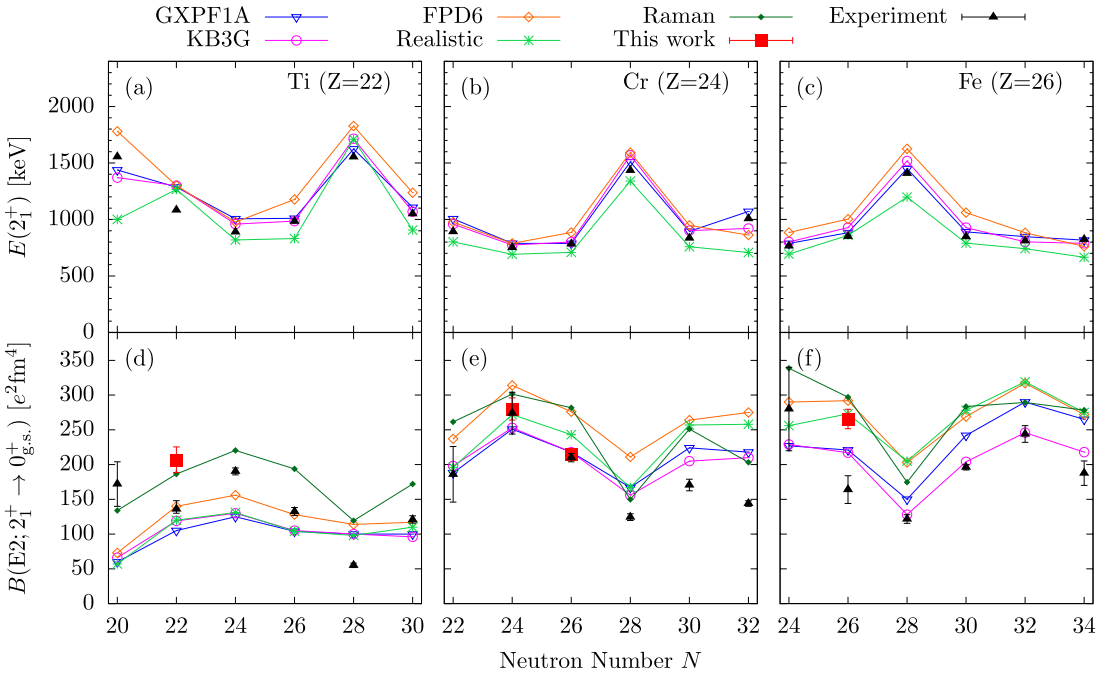


**Fig. 4.** (Color online.) Experimental and theoretical $2_1^+$ excitation energies (a, b, c) and $B(E2)$ values of the $2_1^+ \rightarrow 0_{g.s.}^+$ transition (d, e, f). Both values are plotted against the neutron number for (a, d) titanium, (b, e) chromium, and (c, f) iron isotopes, respectively. $B(E2)$ values from this work are given in red squares. Previously adopted $B(E2)$ values (black triangles) are taken from Refs. [8,9]. The global best fit given by Raman et al. [38] is presented by dark green diamonds. Moreover, shell-model calculations employing the GXPF1A (blue open triangles), KB3G (purple open circles), and FPD6 (orange open diamonds) interactions, as well as a shell-model calculation using a realistic effective Hamiltonian (green stars) are shown.

arise from the lack of precise knowledge of the stopping power, unknown feeding contributions, and the decreasing sensitivity of the DSAM for lifetimes longer than 1 ps. As stated above, the previous $B(E2)$ value is lower than the value for the $N = 20$ isotope $^{42}$Ti and does not match the expectation along the titanium isotopic chain. The new larger $B(E2)$ value for $^{44}$Ti resolves the discrepancy (cf. Fig. 4(d)) and a more collective behavior than in the neighboring semi-magic even–even nucleus $^{42}$Ti is suggested.

For $^{48}$Cr the reduced transition probability of $B(E2; 2_1^+ \rightarrow 0_{g.s.}^+) = 279^{+17}_{-15}\, e^2\,\mathrm{fm}^4$ deduced in this work agrees well with the previously adopted value $B(E2; 2_1^+ \rightarrow 0_{g.s.}^+) = 274(30)\, e^2\,\mathrm{fm}^4$ from Ref. [8]. The adopted value includes the results from Refs. [11–13]. The relative uncertainty can now be further reduced and amounts to 5.8%. The value follows nicely the overall tendency along the chromium isotopes (cf. Fig. 4(e)) with its maximum value at mid-shell.

In $^{52}$Fe there is a discrepancy between the new $B(E2; 2_1^+ \rightarrow 0_{g.s.}^+) = 265^{+15}_{-13}\, e^2\,\mathrm{fm}^4$ value and the previously measured $B(E2; 2_1^+ \rightarrow 0_{g.s.}^+) = 163\,(20)\, e^2\,\mathrm{fm}^4$ value by Yurkewicz et al. [14] (cf. Fig. 4(f)), suggesting a significantly stronger collectivity at $N = Z = 26$. While a small $B(E2)$ value at the $N = 28$ shell closure is expected, a clearly increased $B(E2)$ value in $^{52}$Fe, like it is reported here, cannot be excluded. The difference of both experimental values for $^{52}$Fe is subject of theoretical discussion presented below.

In summary, the new $B(E2; 2_1^+ \rightarrow 0_{g.s.}^+)$ values in $^{44}$Ti and $^{52}$Fe are significantly larger than previously measured, corroborating enhanced collectivity close to the doubly-magic nuclei $^{40}$Ca and $^{56}$Ni at $N = Z$. For Ti and Cr, the $N = Z$ nuclei show largest $B(E2)$ values in comparison to the neighboring even–even isotopes, while for the Fe isotopes, the values at $N = Z$ for $^{52}$Fe and the lighter mid-shell neighbor $^{50}$Fe are comparable within the experimental uncertainties.

For the theoretical description of the excitation energy of the $2_1^+$ states and the new $B(E2; 2_1^+ \rightarrow 0_{g.s.}^+)$ values, shell-model calculations were performed along the isotopic chains of Ti, Cr, and Fe for a wide range where experimental data on $B(E2; 2_1^+ \rightarrow 0_{g.s.}^+)$ values were accessible. The NuShellX@MSU code [31] was employed using three already established interactions for comparison with the present experimental data: FPD6 [15], KB3G [16], and GXPF1A [17]. The model space comprises the $f_{7/2}$, $p_{3/2}$, $p_{1/2}$, and $f_{5/2}$ orbitals, coupled to a $^{40}$Ca core. Effective charges $e_\pi = 1.5\, e$ and $e_\nu = 0.5\, e$ were used for protons and neutrons, respectively. The calculated $B(E2)$ values for the nuclei of interest agree with published calculations employing the FPD6 and GXPF1 interactions [32,33].

In addition, realistic shell-model calculations, using the shell-model code Antoine [34], have been performed. The two-body matrix elements of the residual interaction were derived from many-body perturbation theory, including all diagrams up to third-order in the perturbative expansion of the effective shell-model Hamiltonian [35]. Effective operators to calculate the electromagnetic transition rates have been consistently derived within this perturbative approach. The starting realistic nucleon–nucleon potential is a low-momentum potential derived from the CD-Bonn potential [36] within the $V_{\mathrm{low-k}}$ approach, and using a cutoff momentum $\Lambda = 2.6\,\mathrm{fm}^{-1}$ [37]. The single-proton and single-neutron energies have been chosen to reproduce the excitation energies of single-particle states in $^{57}$Cu and $^{49}$Ca, respectively, and to reproduce the odd-even mass difference around $^{56}$Ni and $^{48}$Ca. Consequently, two-body matrix elements of the residual interaction and effective electromagnetic operators are derived from theory, while single-particle energies are taken from experiment. The $B(E2; 2_1^+ \rightarrow 0_{g.s.}^+)$ values from all four calculations are reported in Table 2.

Along the chain of titanium isotopes, there is only poor agreement between the experimental and theoretical $B(E2; 2_1^+ \rightarrow 0_{g.s.}^+)$ values for all interactions (see Fig. 4(d)). A strong discrepancy is observed for $N = 20$ to 24 due to small theoretical results. This derivation decreases with the increasing number of neutrons to-

ward $N = 26$. At the shell closure at $N = 20$ a factor of three difference is obtained; and the new experimental value for $^{44}$Ti is approximately a factor of two higher than the calculated value. The $N = 26, 30$ values are reproduced quite well. However, at the $N = 28$ sub-shell closure the experimental result of a small $B(E2)$ value is not reproduced by the calculations.

A recent study in the neighboring even–even isotone $^{42}$Ca showed a similar result [7]. Enhanced $B(E2; 2_1^+ \rightarrow 0_{g.s.}^+)$ values were measured in contrast to lower shell-model results. It was suggested by Ref. [39] that the experimental enhancement arises from $2\hbar\omega$ sd-shell excitations, which are not included in the *fp* model space. In addition, a sizable quadrupole moment of the $2_1^+$ state in $^{42}$Ca is proposed to originate from a mixing of the $2_1^+$ state with a superdeformed $2_2^+$ state [7]. In $^{44}$Ti a mixing of the $2_1^+$ state with non-yrast $2^+$ states will have a minor effect due to larger level-energy differences. Thus, the underestimated transition probability is most likely caused by core excitations from the *sd* shell. Furthermore, an overestimated theoretical excitation energy of the $2_1^+$ state is obtained. Neglecting core excitations, the different shell-model calculations predict the energy of the $2_1^+$ state to be $E(2^+) = 1266$ to 1300 keV which exceeds the experimentally observed $E(2^+) = 1083$ keV (cf. Fig. 4 (a)).

The importance of core excitations north-east of $^{40}$Ca is also essential in the schematic $\alpha$-cluster model discussed by Ohkubo et al. [23]. Excitation energies of all rotational bands in $^{44}$Ti are reproduced using an $\alpha + ^{40}\mathrm{Ca}(I^\pi)$ system. Moreover, $B(E2)$ values were determined for the low-lying bands and yield $B(E2; 2_1^+ \rightarrow 0_{g.s.}^+) = 18$ W.u. [23] which reproduces the present experimental value of $B(E2) = 22(2)$ W.u. best.

The different shell-model calculations follow the measured $B(E2)$ systematics for $N < 28$ in the chromium isotopic chain as shown in Fig. 4(e). Deviations are visible only for the FPD6 interaction, which tends to larger $B(E2)$s than experimentally determined. The GXPF1A and KB3G interactions as well as the realistic one are in good agreement with the experimental data at $N < 28$. For $N \geq 28$ the transition strength is overestimated by theory. Especially, the experimental data can hardly be reproduced at the (sub-)shell closures $N = 28$ and $N = 32$.

The comparison between experiment and theory shows only partial agreement for the iron isotopes (see Fig. 4(f)). While the $B(E2)$ values for the two lightest isotopes at $N = 24, 26$, which are calculated within the realistic scheme and the FPD6 interaction, are in a good agreement with the new experimental data, the values from GXPF1A and KB3G calculations are too small. However, the latter two interactions reproduce nicely the values for $N \geq 28$. It is noteworthy, that no calculation describes the huge experimental difference of $\sim 143\, e^2\,\mathrm{fm}^4$ between $N = Z = 26$ and the shell closure at $N = 28$; it is underestimated by all interactions.

Experimental and theoretical $B(E2; 2_1^+ \rightarrow 0_{g.s.}^+)$ values for the even–even $N = Z$ nuclei are shown in Fig. 5. For the doubly-magic $^{56}$Ni at $N = Z = 28$, each of the employed four shell-model interactions overestimate the experimental $B(E2)$ value from Ref. [40]. The global best fit of Raman et al. [38] is in agreement with the new values.

The present $B(E2; 2_1^+ \rightarrow 0_{g.s.}^+)$ values allow for a refined assessment of the aforementioned $B_{4/2}$ values in these isotopes which are shown in Table 3. For the $B_{4/2}$ ratios the following data were taken: (i) The adopted $B(E2; 2_1^+ \rightarrow 0_{g.s.}^+)$ values from Ref. [8] and $B(E2; 4_1^+ \rightarrow 2_1^+)$ values from Refs. [41–43] are used to determine the $B_{4/2}$ ratios (labeled Previous). (ii) The new $B(E2; 2_1^+ \rightarrow 0_{g.s.}^+)$ values from Table 2 are combined with values from Refs. [41–43] (labeled Present). The corresponding $R_{4/2} = E(4_1^+)/E(2_1^+)$ ratio is also summarized in Table 3.

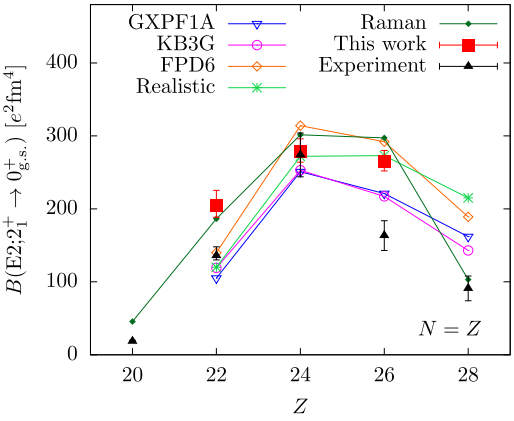


**Fig. 5.** (Color online.) $B(E2; 2_1^+ \rightarrow 0_{g.s.}^+)$ values for even–even $N = Z$ nuclei between $^{40}$Ca and $^{56}$Ni. Same color code as in Fig. 4 is used. See text for details.

**Table 3**
$B_{4/2}$ and $R_{4/2}$ ratios for $^{44}$Ti, $^{48}$Cr, and $^{52}$Fe. Geometrical limits are $B_{4/2} = R_{4/2} = 2.0$ for an ideal vibrator, $B_{4/2} = 1.43$ and $R_{4/2} = 3.33$ for an ideal rotor and $B_{4/2} = 1$ as well as $R_{4/2} < 2$ for a non-collective behavior. See text for details.

| Isotope | $B_{4/2}$ | | $R_{4/2}$ |
|---|---|---|---|
| | Present | Previous | |
| $^{44}$Ti | $1.36^{+0.29}_{-0.22}$ | $2.04^{+0.42}_{-0.32}$ | 2.27 |
| $^{48}$Cr | $1.00^{+0.11}_{-0.08}$ | $1.02^{+0.16}_{-0.14}$ | 2.47 |
| $^{52}$Fe | $1.14^{+0.32}_{-0.21}$ | $1.83^{+0.57}_{-0.38}$ | 2.81 |

The present $B_{4/2}$ ratios for $^{44}$Ti and $^{52}$Fe differ distinctively from the previous results. For both isotopes the former results indicate a vibrator-like behavior, whereas the new $B_{4/2}$ ratios are reduced. The $B_{4/2} = 1.36^{+0.29}_{-0.22}$ in $^{44}$Ti suggests a rotational behavior. In $^{52}$Fe the $B_{4/2} = 1.14^{+0.32}_{-0.21}$ ratio lies between the rotor and the single-particle limit. The ratio given for $^{48}$Cr remains nearly unchanged with a new value $B_{4/2} = 1.00^{+0.11}_{-0.08}$ which is at the limit for a collective behavior. The observed fluctuations which were discussed for the previous $B_{4/2}$ ratios in Ref. [10] are not confirmed.

Moreover, the comparison of $R_{4/2}$ and $B_{4/2}$ ratios does not allow a consistent description. While the $R_{4/2}$ ratios suggest a transition from vibrational to rotational character, the new $B_{4/2}$ ratios show collective behavior with similarities to a rotational motion. Nonetheless, it has to be noted that the $B_{4/2}$ ratios depend also on the $B(E2; 4_1^+ \rightarrow 2_1^+)$ values which were not subject of this work. Especially for $^{44}$Ti, but also for $^{52}$Fe, these values are only known with considerable uncertainties.

## 5. Summary

To summarize, lifetimes in the self-conjugated nuclei $^{44}$Ti, $^{48}$Cr, and $^{52}$Fe were measured with the RDDS method and precise reduced transition probabilities for the $2_1^+$ ground-state transition were determined. The present results yield clearly increased $B(E2; 2_1^+ \rightarrow 0_{g.s.}^+)$ values than previously known for $^{44}$Ti and $^{52}$Fe in the vicinity of two doubly-magic nuclei. The new results indicate enhanced collectivity for all investigated $N = Z$ nuclei. The deduced $B_{4/2}$ ratio suggests a rotational behavior for $^{44}$Ti.

The comparison with state-of-the-art shell-model calculations shows an ambiguous outcome; none of the four effective interactions reproduces all known $B(E2; 2_1^+ \rightarrow 0_{g.s.}^+)$ values from $^{40}$Ca to $^{56}$Ni in a consistent way. There is a strong evidence that the

observed discrepancy between experiment and theory for $^{44}$Ti is related to multi-particle-hole cross-shell configurations similar to recent observations in the neighboring isotone $^{42}$Ca. Also the possible rotational character of $^{44}$Ti could be explained by particle-hole *sd*-shell core excitations which are typically related to a deformed nucleus. At mid $f_{7/2}$ shell, the different calculations reproduce the experimental $B$(E2) values for $^{48}$Cr. Here, the reduced $B_{4/2}$ ratio close to unity remains an open question. The agreement is reduced for $^{52}$Fe; the calculations applying the FPD6 interaction and the effective shell-model Hamiltonian reproduce well the measured $B$(E2) values. At the $N = Z = 28$ shell closure $^{56}$Ni the $B$(E2) values are overestimated by all considered interactions.

Therefore, on the theory side, challenging future shell-model calculations, which include core excitations from the *sd* shell, are needed to resolve the open questions and to obtain a consistent description of the mass region including also the isotopic evolution where even larger discrepancies exist currently, while on the experimental side, improved lifetime measurements of higher-lying states, especially the $4_1^+$ and other members of the ground-state band are of high importance.

## Acknowledgement

A.V. acknowledges support from the Bonn-Cologne Graduate School of Physics and Astronomy (BCGS).

## References

[1] R.B. Huber, W. Kutschera, C. Signorini, P. Blasi, Gamma transitions in $^{44}$Ti and $^{48}$Cr from heavy ion induced reactions, J. Phys., Colloq. 32 (1971) C6-207–C6-208.

[2] W.R. Dixon, R.S. Storey, J.J. Simpson, Lifetimes of $^{44}$Ti levels, Nucl. Phys. A 202 (3) (1973) 579–592.

[3] S. Schielke, K.-H. Speidel, O. Kenn, J. Leske, N. Gemein, M. Offer, Y.Y. Sharon, L. Zamick, J. Gerber, P. Maier-Komor, First measurement and shell model interpretation of the $g$ factor of the $2_1^+$ state in self-conjugate radioactive $^{44}$Ti, Phys. Lett. B 567 (3–4) (2003) 153–158.

[4] R. Hartmann, H. Grawe, K. Kändler, The $\gamma$-decay of $^{42}$Sc and $^{42}$Ti, Nucl. Phys. A 203 (2) (1973) 401–413.

[5] C.D. O'Leary, M.A. Bentley, B.A. Brown, D.E. Appelbe, R.A. Bark, D.M. Cullen, S. Ertürk, A. Maj, A.C. Merchant, Nonyrast high-spin states in $N = Z$ $^{44}$Ti, Phys. Rev. C 61 (2000) 064314.

[6] D.C. Zheng, L. Zamick, D. Berdichevsky, Superdeformed many-particle–many-hole states in $N = Z$ nuclei: beyond the 8p–8h state in $^{40}$Ca, Phys. Rev. C 42 (1990) 1004–1008.

[7] K. Hadyńska-Klęk, P.J. Napiorkowski, M. Zielińska, J. Srebrny, A. Maj, F. Azaiez, J.J. Valiente Dobón, M. Kicińska Habior, F. Nowacki, H. Naïdja, B. Bounthong, T.R. Rodríguez, G. de Angelis, T. Abraham, G. Anil Kumar, D. Bazzacco, M. Bellato, D. Bortolato, P. Bednarczyk, G. Benzoni, L. Berti, B. Birkenbach, B. Bruyneel, S. Brambilla, F. Camera, J. Chavas, B. Cederwall, L. Charles, M. Ciemała, P. Cocconi, P. Coleman-Smith, A. Colombo, A. Corsi, F.C.L. Crespi, D.M. Cullen, A. Czermak, P. Désesquelles, D.T. Doherty, B. Dulny, J. Eberth, E. Farnea, B. Fornal, S. Franchoo, A. Gadea, A. Giaz, A. Gottardo, X. Grave, J. Grębosz, A. Görgen, M. Gulmini, T. Habermann, H. Hess, R. Isocrate, J. Iwanicki, G. Jaworski, D.S. Judson, A. Jungclaus, N. Karkour, M. Kmiecik, D. Karpiński, M. Kisieliński, N. Kondratyev, A. Korichi, M. Komorowska, M. Kowalczyk, W. Korten, M. Krzysiek, G. Lehaut, S. Leoni, J. Ljungvall, A. Lopez-Martens, S. Lunardi, G. Maron, K. Mazurek, R. Menegazzo, D. Mengoni, E. Merchán, W. Męczyński, C. Michelagnoli, J. Mierzejewski, B. Million, S. Myalski, D.R. Napoli, R. Nicolini, M. Niikura, A. Obertelli, S.F. Özmen, M. Palacz, L. Próchniak, A. Pullia, B. Quintana, G. Rampazzo, F. Recchia, N. Redon, P. Reiter, D. Rosso, K. Rusek, E. Sahin, M.-D. Salsac, P.-A. Söderström, I. Stefan, O. Stézowski, J. Styczeń, C. Theisen, N. Toniolo, C.A. Ur, V. Vandone, R. Wadsworth, B. Wasilewska, A. Wiens, J.L. Wood, K. Wrzosek-Lipska, M. Zięblíński, Superdeformed and triaxial states in $^{42}$Ca, Phys. Rev. Lett. 117 (2016) 062501.

[8] B. Pritychenko, M. Birch, B. Singh, M. Horoi, Tables of E2 transition probabilities from the first $2^+$ states in even–even nuclei, At. Data Nucl. Data Tables 107 (2016) 1–139.

[9] M. Seidlitz, P. Reiter, A. Dewald, O. Möller, B. Bruyneel, S. Christen, F. Finke, C. Fransen, M. Górska, H. Grawe, A. Holler, G. Ilie, T. Kotthaus, P. Kudejová, S.M. Lenzi, S. Mandal, B. Melon, D. Mücher, J.-M. Regis, B. Saha, P. von Brentano, A. Wiens, K.O. Zell, Precision lifetime measurements of the first $2^+$ and $4^+$ states in $^{56}$Cr at the $N = 32$ subshell closure, Phys. Rev. C 84 (2011) 034318.

[10] D. Hertz-Kintish, L. Zamick, S.J.Q. Robinson, $B(E2, 4 \to 2)/B(E2, 2 \to 0)$ ratio in even–even nuclei: apparent anomalous behavior of the chromium isotopes, Phys. Rev. C 90 (2014) 034307.

[11] W. Kutschera, R.B. Huber, C. Signorini, P. Blasi, Gamma-ray spectroscopy of $^{48}$Cr, Nucl. Phys. A 210 (3) (1973) 531–543.

[12] B. Haas, P. Taras, J.C. Merdinger, R. Vaillancourt, Yrast states in $^{48}$Cr and reaction mechanism of the $^{34}$S + $^{16}$O reaction at $E_{\text{lab}} = 30$–36 MeV, Nucl. Phys. A 238 (2) (1975) 253–268.

[13] L.P. Ekström, G.D. Jones, F. Kearns, T.P. Morrison, O.M. Mustaffa, D.N. Simister, H.G. Price, P.J. Twin, R. Wadsworth, N.J. Ward, Gamma-ray spectroscopy on $^{48}$Cr, J. Phys. G 5 (6) (1979) 803.

[14] K.L. Yurkewicz, D. Bazin, B.A. Brown, C.M. Campbell, J.A. Church, D.-C. Dinca, A. Gade, T. Glasmacher, M. Honma, T. Mizusaki, W.F. Mueller, H. Olliver, T. Otsuka, L.A. Riley, J.R. Terry, Intermediate-energy Coulomb excitation of $^{52}$Fe, Phys. Rev. C 70 (2004) 034301.

[15] W.A. Richter, M.G. Van Der Merwe, R.E. Julies, B.A. Brown, New effective interactions for the 0f1p shell, Nucl. Phys. A 523 (2) (1991) 325–353.

[16] A. Poves, J. Sánchez-Solano, E. Caurier, F. Nowacki, Shell model study of the isobaric chains $A = 50$, $A = 51$ and $A = 52$, Nucl. Phys. A 694 (1–2) (2001) 157–198.

[17] M. Honma, T. Otsuka, B.A. Brown, T. Mizusaki, Shell-model description of neutron-rich pf-shell nuclei with a new effective interaction GXPF1, Eur. Phys. J. A 25 (1) (2005) 499–502.

[18] S. Frauendorf, A.O. Macchiavelli, Overview of neutron–proton pairing, Prog. Part. Nucl. Phys. 78 (2014) 24–90.

[19] C. Qi, R. Wyss, N = Z nuclei: a laboratory for neutron–proton collective mode, Phys. Scr. 91 (1) (2016) 013009.

[20] M. Honma, T. Otsuka, B.A. Brown, T. Mizusaki, New effective interaction for $pf$-shell nuclei and its implications for the stability of the $N = Z = 28$ closed core, Phys. Rev. C 69 (2004) 034335.

[21] K. Kaneko, Y. Sun, G. de Angelis, Enhancement of high-spin collectivity in $N = Z$ nuclei by the isoscalar neutron–proton pairing, Nucl. Phys. A 957 (2017) 144–153.

[22] B. Cederwall, F.G. Moradi, T. Bäck, A. Johnson, J. Blomqvist, E. Clément, G. de France, R. Wadsworth, K. Andgren, K. Lagergren, A. Dijon, G. Jaworski, R. Liotta, C. Qi, B.M. Nyakó, J. Nyberg, M. Palacz, H. Al-Azri, A. Algora, G. de Angelis, A. Ataç, S. Bhattacharyya, T. Brock, J.R. Brown, P. Davies, A. Di Nitto, Z. Dombrádi, A. Gadea, J. Gál, B. Hadinia, F. Johnston-Theasby, P. Joshi, K. Juhász, R. Julin, A. Jungclaus, G. Kalinka, S.O. Kara, A. Khaplanov, J. Kownacki, G. La Rana, S.M. Lenzi, J. Molnár, R. Moro, D.R. Napoli, B.S.N. Singh, A. Persson, F. Recchia, M. Sandzelius, J.-N. Scheurer, G. Sletten, D. Sohler, P.-A. Söderström, M.J. Taylor, J. Timár, J.J. Valiente-Dobón, E. Vardaci, S. Williams, Evidence for a spin-aligned neutron–proton paired phase from the level structure of $^{92}$Pd, Nature 469 (7328) (2011) 68–71.

[23] S. Ohkubo, Y. Hirabayashi, T. Sakuda, $\alpha$-cluster structure of $^{44}$Ti in core-excited $\alpha$ + $^{40}$Ca model, Phys. Rev. C 57 (1998) 2760–2762.

[24] M. Kimura, H. Horiuchi, Coexistence of cluster structure and superdeformation in $^{44}$Ti, Nucl. Phys. A 767 (2006) 58–80.

[25] J. Ljungvall, A. Görgen, M. Girod, J.-P. Delaroche, A. Dewald, C. Dossat, E. Farnea, W. Korten, B. Melon, R. Menegazzo, A. Obertelli, R. Orlandi, P. Petkov, T. Pissulla, S. Siem, R.P. Singh, J. Srebrny, C. Theisen, C.A. Ur, J.J. Valiente-Dobón, K.O. Zell, M. Zielińska, Shape coexistence in light Se isotopes: evidence for oblate shapes, Phys. Rev. Lett. 100 (2008) 102502.

[26] W. Rother, A. Dewald, H. Iwasaki, S.M. Lenzi, K. Starosta, D. Bazin, T. Baugher, B.A. Brown, H.L. Crawford, C. Fransen, A. Gade, T.N. Ginter, T. Glasmacher, G.F. Grinyer, M. Hackstein, G. Ilie, J. Jolie, S. McDaniel, D. Miller, P. Petkov, T. Pissulla, A. Ratkiewicz, C.A. Ur, P. Voss, K.A. Walsh, D. Weisshaar, K.-O. Zell, Enhanced quadrupole collectivity at $N = 40$: the case of neutron-rich Fe isotopes, Phys. Rev. Lett. 106 (2011) 022502.

[27] T. Braunroth, A. Dewald, H. Iwasaki, S.M. Lenzi, M. Albers, V.M. Bader, T. Baugher, T. Baumann, D. Bazin, J.S. Berryman, C. Fransen, A. Gade, T. Ginter, A. Gottardo, M. Hackstein, J. Jolie, A. Lemasson, J. Litzinger, S. Lunardi, T. Marchi, V. Modamio, C. Morse, D.R. Napoli, A. Nichols, F. Recchia, S.R. Stroberg, R. Wadsworth, D. Weisshaar, K. Whitmore, K. Wimmer, Reduced transition strengths of low-lying yrast states in chromium isotopes in the vicinity of $N = 40$, Phys. Rev. C 92 (2015) 034306.

[28] K. Kolos, D. Miller, R. Grzywacz, H. Iwasaki, M. Al-Shudifat, D. Bazin, C.R. Bingham, T. Braunroth, G. Cerizza, A. Gade, A. Lemasson, S.N. Liddick, M. Madurga, C. Morse, M. Portillo, M.M. Rajabali, F. Recchia, L.L. Riedinger, P. Voss, W.B. Walters, D. Weisshaar, K. Whitmore, K. Wimmer, J.A. Tostevin, Direct lifetime measurements of the excited states in $^{72}$Ni, Phys. Rev. Lett. 116 (2016) 122502.

[29] A. Dewald, O. Möller, P. Petkov, Developing the recoil distance Doppler-shift technique towards a versatile tool for lifetime measurements of excited nuclear states, Prog. Part. Nucl. Phys. 67 (3) (2012) 786–839.

[30] F. Brandolini, S.M. Lenzi, D.R. Napoli, R.V. Ribas, H. Somacal, C.A. Ur, D. Bazzacco, J.A. Cameron, G. de Angelis, M.D. Poli, C. Fahlander, A. Gadea, S. Lunardi, G. Martínez-Pinedo, N.H. Medina, C.R. Alvarez, J. Sánchez-Solano, C.E. Svensson, Precise DSAM lifetime measurements in $^{48}$Cr and $^{50}$Cr as a test of large scale shell model calculations, Nucl. Phys. A 642 (3–4) (1998) 387–406.

[31] B.A. Brown, W.D.M. Rae, The Shell-model code NuShellX@MSU, Nucl. Data Sheets 120 (2014) 115–118.
[32] S.J.Q. Robinson, T. Hoang, L. Zamick, A. Escuderos, Y.Y. Sharon, Shell model calculations of $B(E2)$ values, static quadrupole moments, and $g$ factors for a number of $N = Z$ nuclei, Phys. Rev. C 89 (2014) 014316.
[33] L. Zamick, Y.Y. Sharon, S.J.Q. Robinson, M. Harper, Consequences of omitting spin-orbit partner configurations for $B(E2)$ values and quadrupole moments in nuclei, Phys. Rev. C 91 (2015) 064321.
[34] E. Caurier, G. Martínez-Pinedo, F. Nowacki, A. Poves, A.P. Zuker, The shell model as a unified view of nuclear structure, Rev. Mod. Phys. 77 (2005) 427–488.
[35] L. Coraggio, A. Covello, A. Gargano, N. Itaco, T.T.S. Kuo, Effective shell-model Hamiltonians from realistic nucleon–nucleon potentials within a perturbative approach, Ann. Phys. 327 (9) (2012) 2125–2151.
[36] R. Machleidt, High-precision, charge-dependent Bonn nucleon–nucleon potential, Phys. Rev. C 63 (2001) 024001.
[37] S. Bogner, T.T.S. Kuo, L. Coraggio, A. Covello, N. Itaco, Low momentum nucleon–nucleon potential and shell model effective interactions, Phys. Rev. C 65 (2002) 051301.
[38] S. Raman, C.W. Nestor Jr., P. Tikkanen, Transition probability from the ground to the first-excited $2^+$ state of even–even nuclides, At. Data Nucl. Data Tables 78 (1) (2001) 1–128.
[39] B.A. Brown, The nuclear shell model towards the drip lines, Prog. Part. Nucl. Phys. 47 (2) (2001) 517–599.
[40] K.L. Yurkewicz, D. Bazin, B.A. Brown, C.M. Campbell, J.A. Church, D.C. Dinca, A. Gade, T. Glasmacher, M. Honma, T. Mizusaki, W.F. Mueller, H. Olliver, T. Otsuka, L.A. Riley, J.R. Terry, Nuclear structure in the vicinity of $N = Z = 28$ $^{56}$Ni, Phys. Rev. C 70 (2004) 054319.
[41] J. Chen, B. Singh, J.A. Cameron, Nuclear data sheets for $A = 44$, Nucl. Data Sheets 112 (9) (2011) 2357–2495.
[42] T.W. Burrows, Nuclear data sheets for $A = 48$, Nucl. Data Sheets 107 (7) (2006) 1747–1922.
[43] Y. Dong, H. Junde, Nuclear data sheets for $A = 52$, Nucl. Data Sheets 128 (2015) 185–314.